Case Studies in Thermal Engineering 26 (2021) 100967

Contents lists available at ScienceDirect

Case Studies in Thermal Engineering

journal homepage: www.elsevier.com/locate/csite

On the effects of orientation on flow and heat transfer from a semi-circular cylinder near a stationary wall

Rajendra S. Rajpoot [a], K. Anirudh [a,b], S. Dhinakaran [a,*]

[a] The Centre for Fluid Dynamics, Department of Mechanical Engineering, Indian Institute of Technology Indore, Khandwa Road, Simrol, Indore, 453 552, India

[b] Department of Mechanical Engineering, School of Technology, Pandit Deendayal Energy University, Raisan, Gandhinagar, 382 426, India

ARTICLE INFO

Keywords:
Semi-circular cylinder
Stationary wall
Heat transfer
Vortex shedding suppression
Shear flow

ABSTRACT

Numerical analysis of flow and forced convection heat transport from a two-dimensional semi-circular cylinder placed near a stationary wall is presented. The uniformly heated cylinder is within the boundary layer of the plane wall and is subjected to linear shear flow. An unsteady flow of incompressible Newtonian fluid around the cylinder is studied assuming constant properties. Two different orientations of the cylinder, i.e. the curved and flat surfaces exposed to the incoming flow, are considered, and the results are compared with those of a circular cylinder. The cylinder-to-wall gap ratio (G/D.) values are varied between 0.1 and 0.5, and the Reynolds number range of $100 \leq Re \leq 200$ is considered. Numerical experiments are performed using Ansys Fluent. Results suggest that the presence of a stationary wall influences both the flow and thermal fields significantly. A decrement in the drag coefficient and average Nusselt number values is reported, while the lift coefficient and Strouhal number increase, resulting from shear layers' interaction in the gap between cylinder and wall. The heat transfer enhancement ratio is higher for the flow past curved forebody than the flat forebody configuration and circular cylinder. Mean Nusselt number correlations for the range of parameters considered in the present study are provided.

1. Introduction

Hydrodynamics of bluff bodies has intrigued researchers for several decades in the past and continues to stay relevant to the interests of academic and industrial scholars. There is a substantial body of literature devoted to theoretical, experimental, and numerical studies that assert the interesting underlying flow physics. Researchers have always been attracted to the vibrant yet simplistic bluff body flow topic as it has been used occasionally to model complex practical problems. For instance, cylinders with different cross-sections can study a related physical problem involving flow and heat and mass transfer. Semi-circular cylinder, amongst various geometries simulated so far, seems fascinating enough due to the influence of curves and sharp corners on flow and thermal fields. Such a cross-section finds applications in various fields of engineering including thermal cooling [1,2], aerodynamics of road vehicles [3], renewable energy [4–6] and food processing [7] especially in compact heat exchanger [8,9] where better space economy is a major challenge.

The topology of flow structure around a semi-circular cylinder exposed to crossflow offers interesting flow physics. The curved feature provides streamlining effect like a circular cylinder, while the sharp corners resemble the flow structure of a square or

* Corresponding author.
E-mail address: sdhina@iiti.ac.in (S. Dhinakaran).

https://doi.org/10.1016/j.csite.2021.100967
Received 31 October 2020; Received in revised form 23 March 2021; Accepted 25 March 2021
Available online 30 March 2021

Nomenclature

C_D	drag coefficient, $F_D/(0.5\rho U_0^2 D)$
C_L	lift coefficient, $F_L/(0.5\rho U_0^2 D)$
CP	pressure coefficient, $(p - p_0)/(0.5\rho U_0^2)$
C_p	specific heat capacity, $[J/(kgK)]$
D	diameter of the cylinder, $[m]$
f	frequency of vortex shedding cycle, $1/T$
F_D	lift force per unit length, $[N/m]$
F_L	drag force per unit length, $[N/m]$
G	gap height from bottom edge or surface of cylinder to wall, $[m]$
G/D	non-dimensional gap height from cylinder to wall
k	thermal conductivity of fluid, $[W/(mK)]$
L	length of the boundary, $[m]$
M, N	number of grids in x- and y-direction, respectively
Nu	Nusselt number, $-\partial\Theta/\partial n$
P	non-dimensional pressure, $p/(\rho U_0^2)$
p	dimensional pressure, $[N/m^2]$
Pr	Prandtl number, $(\mu C_P)/k$
Re	shear flow based Reynolds number, $(\lambda D^2 \rho)/\mu$
Ri	Richardson number, Gr/Re^2
St	Strouhal number, $(fD)/U_0$
T	time period of vortex shedding
t	dimensional time, $[s]$
U, V	non-dimensional x-component of velocity, (u/U_0), and y-component of velocity, (v/U_0)
u, v	dimensional x- and y-component of velocity, $[m/s]$
U_0	reference horizontal velocity, $[m/s]$
X, Y	non-dimensional horizontal distance, (x/D), vertical distance, (y/D)
x, y	horizontal, vertical distance $[m]$

Greek

λ	slope of the incident velocity profile
μ	dynamic viscosity, $[kg/(ms)]$
ω	vorticity magnitude, $[1/s]$
ρ	density, $[kg/m^3]$
τ	non-dimensional time, $(tU_0)/D$
Θ	non-dimensional temperature, $(\theta - \theta_0)/(\theta_H - \theta_0)$
θ	dimensional temperature, (K)

Subscript

ds	downstream
H	high value
h	height
l	local value
M	mean value
o	reference value
us	upstream

triangular cylinder. Articles detailing the related laminar flow phenomenon are limited in the literature for both confined and unconfined domains. When the fluid flows across an unconfined semi-circular cylinder with curved fore-body facing flow (C1 configuration), at Reynolds number, Re = 0.55–0.60, first flow separation occurs, beyond which symmetric recirculation region appears in the wake region. As Re is increased further, asymmetry develops downstream of the cylinder due to insufficient stability in the wakes, leading to the onset of Bénard-von Kármán vortex shedding process [10]. This transition in flow regime happens at a critical value of Reynolds number, $Re_{cr} = 39.5–40$, wherein the flow becomes unsteady with the periodic shedding of vortices [11]. Compared to other bluff body shapes, this value of Re_{cr} is very less, which usually lies above Re = 40. A prime reason for such a transition is ascertained to lesser streamlining and asymmetry about Y-axis. Further, due to confinement, this critical value is reported to increase up to $Re_{cr} =$ 69–70 for a blockage ratio of 25% [12]. When the flat face of the cylinder (semicircular) is in-line with the horizontal axis, this critical value further rises to $Re_{cr} = 120–130$ [13]. Orienting cylinder at different inclination angles (α) [14] affects flow separation and vortex formation distinctly, while at the singularity points, a leap in Nusselt number is observed. Flow parameters including coefficient of lift (C_L), coefficient of drag (C_D), Strouhal number (St), and mean Nusselt number (Nu_M) decrease with increasing α. Curved and flat

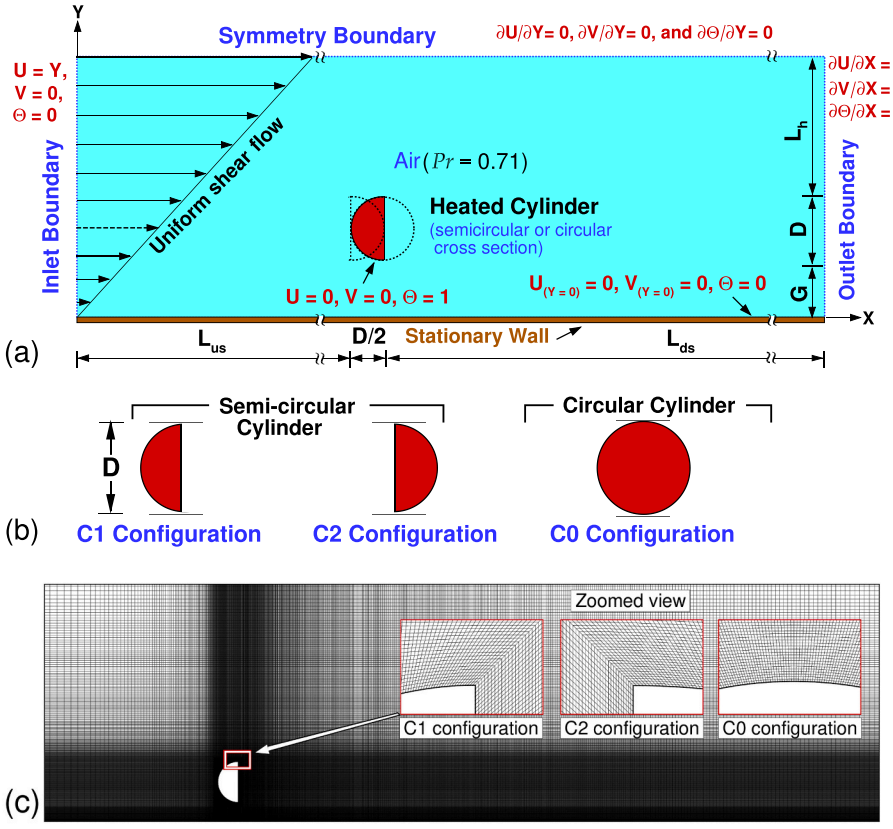

Fig. 1. (*a*) Sketch of the computational domain for uniform shear flow past a heated cylinder placed near a stationary wall with its co-ordinate system and imposed boundary conditions. (*b*) Different configurations of heated cylinder *i.e.*, *C*1, *C*2 and *C*0 are presented for rounded-, flat-forebody semi-circular and circular cross sections, respectively. (*c*) Non-uniform mesh distribution inside the domain at $G/D = 0.5$ with zoomed view of mesh elements clustered around a cylinder for various configurations.

fore-bodies facing incoming flow are often compared for flow and heat transfer phenomena, termed as *C*1 and *C*2 configurations, respectively (shown in Fig. 1). Heat dissipation occurs more from the curved surface of the cylinder when compared with the flat surface for *C*1 configuration [15]. Global flow quantities are of higher value for *C*2 configuration than *C*1, except for *St* and Nu_M [16, 17]. Also, flow and thermal fields are more unstable for *C*1 configuration than *C*2. The thermal buoyancy is seen to introduce further instability, which is severe at lower Re values. In short, the flow and heat transfer characteristics are inconsistent for *C*1 and *C*2 configurations for an unconfined computational domain.

As stated above, flow around complicated shapes is usually perceived through simpler analogous models for comprehending the underlying flow physics. Fluid flow across two-dimensional bluff bodies placed near a stationary wall shares many of these flow features. Such a problem has both fundamental significance in fluid dynamics and practical importance to the industry. The stationary plane wall interferes with the normal velocity profile and acts as a surface for a boundary layer to grow. In applications related to submerged structures like the design of pipelines or submarines and underwater vehicles [18,19], the cylinder may be submerged in a thick boundary layer. In this paper, the cylinder is assumed to be very small and submerged in the boundary layer of the stationary wall. Hence, a linear shear profile at the inlet is implemented, which suffices the assumption. Fundamentally, flow across a long cylinder is disturbed by the presence of a wall in the vicinity. It is well-known that the shedding of vortices is suppressed when the cylinder is very close to the wall. Since vortex shedding causes dynamic loading on structures and its presence is not always desirable, it is vital to study the role of ground effect on suppression vortex shedding. Bhattacharyya and Maiti [20] emphasised that vortex shedding behind the cylinder is influenced by the presence of a stationary wall when Re is taken up to 800, and G/D values are 0, 0.25 and 0.5. Recirculation regions that form on the wall are transported downstream without detaching from the wall as time progresses. In another study [21], the vortex shedding was reported to occur at $G/D = 0.5$, and the corresponding *St* was higher than that for the isolated cylinder case. Due to the consideration of uniform shear profile at the inlet, the drag force experienced by the cylinder decreases with a reduction in G/D values. In contrast, the cylinder experiences a large positive lift. Vortex shedding suppression occurs, and the wake becomes steady at $G/D = 0.25$. In further continuation [22], at $G/D \leq 0.25$ for lower Reynolds number ($Re \leq 500$), vortex shedding is seen to be suppressed, while the wake behind the cylinder remains steady. In other studies [23,24], the dependency of aerodynamic characteristics of flow past a rectangular cylinder at various parameters are discussed, which more or less provide the same inferences. Dipankar and Sengupta [25] provided one of the pioneering numerical results for laminar flow across a circular

cylinder near a stationary wall at Re = 1200 and $G/D = 0.5$ and 1.5. At lower gap ratio values, the interaction between vorticity fields of the cylinder and the wall is found to be paramount, because of which unsteady separation occurs at the wall, causing a high adverse pressure gradient. At high gap ratio values, this pressure gradient decreases, causing separation at the upstream end of the wall. Most importantly, authors advocate that C_D remains indifferent to G/D variation until the gap falls near the thickness of the boundary layer on the plane wall. Kumaran and Vengadesan [26] performed numerical experiments to study three-dimensional laminar flow across a rectangular cylinder near a wall at Re = 450 and gap ratio values from 1.5 to 0.2. They reported that periodic activities of wake are disturbed due to the wall presence, suppressing the vortex shedding completely. The interaction of shear layers from the bottom and top side of the cylinder results in the mitigation of shedding. Singha et al. [27] carried out finite-difference simulations for circular cylinder near a plane wall at Re = 20–200 and $G/D = 0.1$–2.5. At low values of G/D, vortex shedding was found to occur only from above the cylinder. In contrast, a jetting action occurred from the beneath, resulting in an overall heat transfer increase. However, the Nusselt number decreases after a critical gap ratio value between 0.2 and 0.3. Scandura et al. [28] compared two- and three-dimensional vorticity dynamics of flow across a bluff body in the vicinity of the wall. Computations were performed at Reynolds number values of Re = 200 and 500. From the numerical results, the authors explained that 2D analysis for the considered case was sufficient, as many variations amongst 2D and 3D numerical results are not seen for moderate G/D ratio values. Mahir [29] also compared flow across a square cylinder in ground effect for two- and three-dimensional domains. They realised that the primary vortex structure remains almost the same for both 2D and 3D domains. At the same time, 3D configuration predicts a lower mean drag coefficient and the root-mean-square of lift coefficient values than the 2D case. Kumar and Dhiman [30] studied laminar cross-buoyant flow around a square cylinder placed near a stationary wall at Re = 1–100, $Ri = 0$–2 and various gap ratios (G/D) values from 0.25 to 2. At $Ri = 0$, they found the flow to remain steady for $G/D = 0.25$–0.5, and unsteadiness is seen for $G/D = 1$ at $Re_{cr} = 55$.

From the above literature survey is clear that sufficient information is available for flow across the confined and unconfined semi-circular cylinder. Further, flow and heat transfer from various bluff body shapes placed near a stationary wall is also well-explored. However, flow and forced convection heat transfer from a semi-circular cylinder in the laminar cross-flow regime is missing. Although, (Kumarasamy and Barlow) [31,32] have studied only fluid flow (not heat transfer) around a semi-circular cylinder in the vicinity of stationary as well as moving wall, the considered range of Re values is very high, and it falls in turbulent flow regime. Also, Kumar *et al.* [33], have studied forced convection heat transfer from a hot semi-circular cylinder. However, in their study, the cylinder is in a confined domain filled with power-law fluids. The present study is carried out to shed some light on the fundamental knowledge of flow separation, vorticity dynamics and its influence on the heat transfer from the heated cylinder near the plane wall in a laminar unsteady flow regime. Two different orientations (*i.e.*, rounded- and flat-forebody configurations of the same diameter) are considered during numerical computations. Smaller values of cylinder-to-wall gap ratio (*i.e.*, 0.1–0.5) are studied for different values of Reynolds number (*i.e.*, 100–200). As already stated above, it is assumed that the incoming flow at inlet possesses a linear shear profile for modelling the cylinder's placement in the boundary layer of the stationary wall. Also, fluid flow around the cylinder is not always uniform in nature, especially near the wall. Some amount of shear always exists due to the inherent property of fluid and wall roughness at boundaries. However, in most bluff body flow instances in engineering applications, the free-stream condition is taken into account instead of considering a shear profile [34]. Furthermore, insight into the effect of shape variation is provided through a rigorous comparison of semi-circular and circular cylinder flow and thermal fields. The influence of the stationary wall is projected through discrete comparison with unconfined flow situation for various flow conditions.

2. Mathematical formulation

2.1. Problem description

A two-dimensional semi-circular cylinder of diameter D is placed at a certain height G above a stationary wall, as shown in Fig. 1 (a). The cylinder-to-wall gap ratio (G/D) is used as a reference parameter for varying the gap between the cylinder and the wall. A linear shear profile with slope λ is applied to the incoming flow. As an effect of this, the velocity at inlet becomes $U = Y$, while the dimensionless temperature is maintained at $\Theta = 0$. It should be noted that the transverse velocity component is set to be zero at this boundary. The cylinder is kept at a higher temperature than the surrounding fluid, *i.e.* $\Theta = 1$, and a no-slip boundary condition is applied. A symmetry boundary condition is adopted at the top boundary with a zero-gradient condition for temperature. On the stationary wall, the no-slip condition is applied and with temperature fixed to the far-field value. The pressure outlet condition is used at the outlet boundary, which assumes a zero gauge (static) pressure. The default outflow boundary condition of the FLUENT has been used, which implies a zero diffusion flux for all flow variables, similar to Neumann boundary condition ($\partial U/\partial X = 0$, $\partial V/\partial X = 0$ and $\partial \Theta/\partial X = 0$). As depicted in Fig. 1(b), two orientations of the cylinder, namely, $C1$ and $C2$ configurations are studied, wherein the fore-body shape of the cylinder facing incoming flow is different. Artificial boundaries (other than the stationary wall) are placed sufficiently far from the cylinder to avoid any interference on the final results. In the considered range of Reynolds number and gap ratio values, it is safe to assume a two-dimensional approach backed by Scandura et al. [28] and Mahir [29]. For simplifying the problem, it is assumed that the flow is unsteady, laminar, two-dimensional, and incompressible. Thermophysical properties of the wall are taken to be constant concerning the temperature, and roughness on it is neglected. The thermal conductivity of air is assumed to be constant in every direction, and viscous dissipation is not taken into account. The cylinder is assumed to be infinitely long in z - direction, so that it can be modelled two-dimensionally [35].

Table 1
Grid sensitivity and downstream length (L_{ds}) dependence test on time-averaged drag coefficient ($\overline{C}_D$), Strouhal number (St) and mean Nusselt number (Nu_M) at Re = 100, $G/D = 0.5$ and L_{ds}.

L_{ds}	Grid (M×N)	Smallest grid size	$\overline{C}_D$	Relative Deviation (%)	St	Relative Deviation (%)	Nu_M	Relative Deviation (%)
45	A (820×715)	0.010	3.38	6.156	0.29	6.452	6.96	5.177
	B (985×715)	0.005	3.270	2.701	0.296	4.516	6.99	4.768
	C (1150×715)	0.001	3.19	0.188	0.314	1.29	7.29	0.681
55[a]	D (820×740)	0.010	3.23	1.445	0.297	4.194	7.10	3.270
	E (985×740)	0.005	3.187	0.094	0.302	2.581	7.21	1.771
	F (1150×740)[a]	0.001	3.183	0.031	0.311	0.323	7.33	0.136
65	G (820×765)	0.010	3.220	1.131	0.298	3.871	7.22	1.635
	H (985×765)	0.005	3.186	0.063	0.304	1.935	7.26	1.090
	I (1150×765)	0.001	3.184[b]	–	0.31[b]	–	7.34[b]	–

[a] Mesh and downstream length (L_{ds}) used in this study.
[b] Reference data used for the calculation of relative deviation in percentage.

2.2. Governing equations

With the above mentioned assumptions, the flow and heat transfer are modelled by the Navier-Stokes equation, given as Continuity equation:

$$\frac{\partial U}{\partial X}+\frac{\partial V}{\partial Y}=0, \tag{1}$$

Momentum equations:

$$\frac{\partial U}{\partial \tau}+U\frac{\partial U}{\partial X}+V\frac{\partial U}{\partial Y}=-\frac{\partial P}{\partial X}+\frac{1}{Re}\left(\frac{\partial^2 U}{\partial X^2}+\frac{\partial^2 U}{\partial Y^2}\right), \tag{2}$$

$$\frac{\partial V}{\partial \tau}+U\frac{\partial V}{\partial X}+V\frac{\partial V}{\partial Y}=-\frac{\partial P}{\partial Y}+\frac{1}{Re}\left(\frac{\partial^2 V}{\partial X^2}+\frac{\partial^2 V}{\partial Y^2}\right), \text{and} \tag{3}$$

Energy equation:

$$\frac{\partial \Theta}{\partial \tau}+U\frac{\partial \Theta}{\partial X}+V\frac{\partial \Theta}{\partial Y}=\frac{1}{Re.Pr}\left(\frac{\partial^2 \Theta}{\partial X^2}+\frac{\partial^2 \Theta}{\partial Y^2}\right). \tag{4}$$

The above equations are written in the non-dimensional form, and the following scales are used for the non-dimensionalisation:

$$X=\frac{x}{D}, Y=\frac{y}{D}, \tau=\frac{tU_0}{D}, P=\frac{p}{\rho U_0^2}, U=\frac{u}{U_0}, V=\frac{v}{U_0}, \text{and } \Theta=\frac{\theta-\theta_0}{\theta_H-\theta_0}.$$

The other dimensionless variables used above are Reynolds number, $\mathrm{Re}=\frac{\lambda D^2\rho}{\mu}$ and Prandtl number, $\mathrm{Pr}=\frac{\mu C_P}{k}$. Height of the cylinder and reference temperature are indicated by D and θ_0, respectively. Also, U_0 represents the reference velocity. Non-dimensional scales for x-distance, y-distance, time, pressure, x-velocity, y-velocity and temperature are denoted by X, Y, τ, P, U, V and Θ, respectively.

3. Numerical details

Numerical computations are performed using the commercial CFD package ANSYS FLUENT® [36]. FLUENT is based on the control volume technique, and it solves the governing equations in a staggered grid system for structured grids. SIMPLE (Semi-Implicit Method for Pressure-Linked Equations) algorithm [37] is used for solving the governing equations. A pressure-based solver is selected in which the pressure field value is obtained by solving a correction equation obtained through the combination of continuity and momentum equations. For modelling the two-dimensional transient flow, laminar and viscous models with double precision are adopted. An implicit method is selected to get the discretised system of equations. QUICK (Quadratic Upstream Interpolation for Convective Kinematics) scheme is selected for spatial discretisation of the convective and diffusive terms of Eqns. (2)–(4) [38]. PRESTO (staggering pressure option) interpolation technique is used to interpolate calculated pressure on the faces [39]. For transient formulation, a second-order implicit scheme is used. The optimum convergence criteria for the inner (time step) iterations in the unsteady case is set to the value of 10^{-6}.

4. Grid generation and code verification

A visual representation of the grid used in the present study is shown in Fig. 1(b) and details of the structured non-uniform mesh used for computations near the cylinder are given in Fig. 1(c). The top lateral boundary is placed at a distance $L_h = 10D$ from the top edge/surface of the cylinder. The inlet boundary is situated at a distance of $10D$ from the front face of the cylinder, which is also

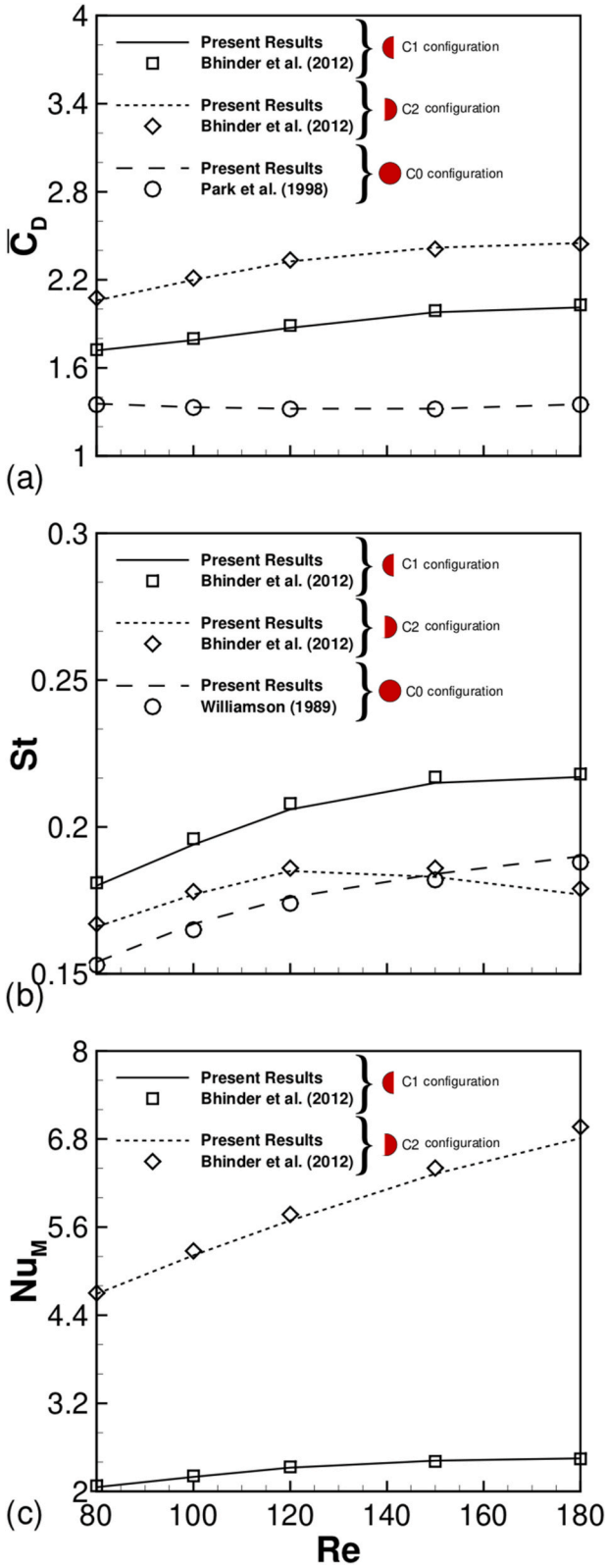

Fig. 2. Comparison of time-averaged drag ($\overline{C}_{D1}$, $\overline{C}_{D2}$ and $\overline{C}_{D0}$), Strouhal number (St) and mean Nusselt number (Nu_M) with the results of Bhinder et al. [14], Williamson [39] and Park et al. [40].

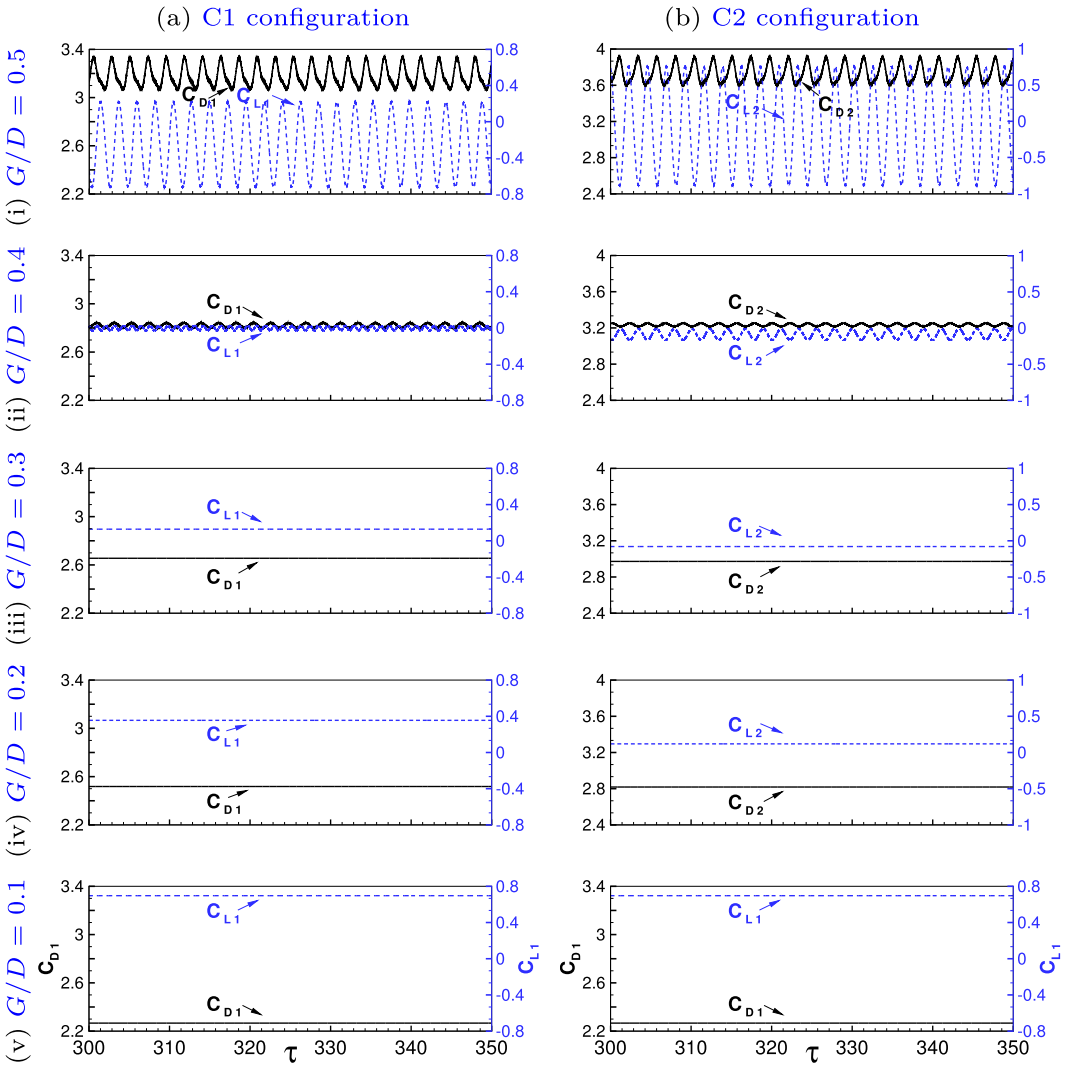

Fig. 3. Time evolution of the drag (C_D, solid line) and lift (C_L, dotted line) coefficients at various cylinder-to-wall gap ratios, G/D at Re = 100 for both cylinder configurations.

referred to as the upstream length, L_{us}. Influence of downstream length, L_{ds}, is significant in comparison to other boundaries, and hence, $\overline{C}_{D1}$ (time-averaged drag coefficient), *St* and *Nu* of the cylinder are tested for three distinct values of downstream length *viz.*, 45*D*, 55*D* and 65*D*. The value of $L_{ds} = 55D$ is found to be apt as no significant variation in parameters are seen between $L_{ds} = 55D$ and 65*D*, making it suitable for further testing of grid choices (Details given in Table 1). Although grid dependence tests are carried out at different G/D values, for the sake of brevity, data are presented only for $G/D = 0.5$, as vortex shedding exists at this particular configuration. Rigorous numerical experiments are performed to check the grid dependency on flow characteristics for various grid sizes for each value of G/D. Nine distinct grids are tested and to capture the fine details of convection phenomenon near the cylinder, a grid size of 0.001*D* is chosen, while elsewhere (except the transition zone) a coarser mesh with an element size of 0.25*D* is adopted. In the transition zone, the grids are drawn between 0.001D and 0.025D for smooth distribution of mesh using different bias factors *i.e.*, (growth rate) $^{(n-1)}$, wherein '*n*' is the number of divisions. The downstream length 55*D* and grid F (1150 × 740) turns out to be an economical choice to capture the best flow features around the semi-circular cylinder while taking computational accuracy and time into consideration. A time step dependence test was also carried out for various values varying from 0.01 to 0.001. For the sake of brevity, the details are left out, but finally, 0.001 is found to be an optimum value. Courant number is maintained at a value less than 0.01 for all cases.

For verifying the computational code used in the present study, extensive numerical code verification tests are performed. Verification is conducted with available works, firstly on flow past a circular cylinder by Williamson (i.e., $St = \frac{-3.3265}{Re} + 0.1816 + 1.6 \times 10^{-4}\, Re$) [40], Park et al. [41] and similarly flow past a semi-circular cylinder by Bhinder et al. [14]. The

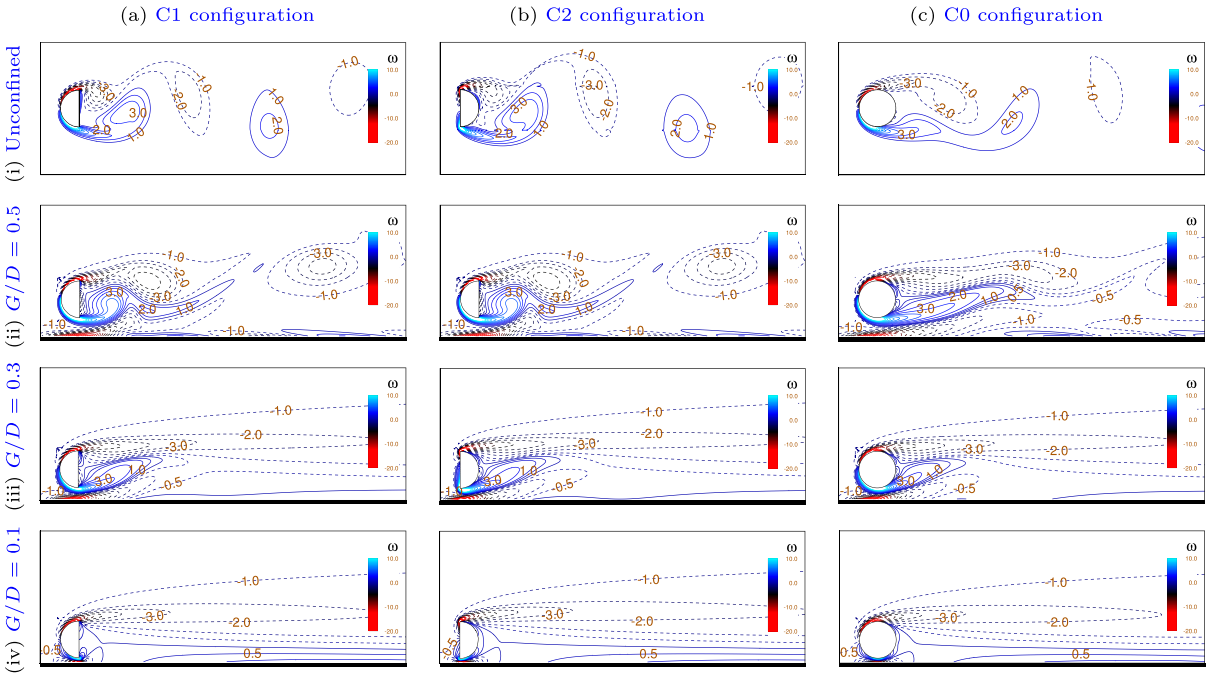

Fig. 4. Instantaneous vorticity contours at different configurations for various values of cylinder-to-wall gap ratio (G/D). The contours are presented at non-dimensional time, $\tau = 300$ and at Reynolds number, $\mathrm{Re} = 100$.

comparison is shown in terms of $\overline{C}_D$, St and Nu_M in Fig. 2. The present computational results is seen to agree well with the published results and the maximum deviation is less than 2.5%.

5. Results and discussion

Numerical computations are carried out to study flow and forced convective heat transfer from a two-dimensional semi-circular cylinder subjected to linear shear flow in the vicinity of a stationary wall. Two distinct orientations of the semi-circular cylinder are focused on, *i.e.* rounded and flat fore-bodies facing the incoming flow and they are named as $C1$ and $C2$ configurations, respectively. The following physical parameters are considered in this study:

- Reynolds number (Re) = 100, 125, 150, and 200.
- Cylinder-to-wall gap ratio (G/D) = 0.1–0.5, in the steps of 0.1.
- Prandtl number (Pr) = 0.71 (as for air).

5.1. Flow characteristics

5.1.1. Time evolution of lift and drag coefficients

In the present study, both steady and unsteady flow regimes can be seen due to a stationary wall. From the literature [21], it can be expected that below a specific critical non-dimensional gap height from cylinder to wall $(G/D)_{cr}$, suppression of vortex shedding occurs. Thereafter the flow must remain steady, and standing asymmetric wake can exist downstream of the cylinder. Time evolution trends for both lift and drag coefficients of $C1$ and $C2$ configurations are given in Fig. 3(a) and (b), respectively. The solid line represents C_D, while the dashed line represents C_L variation. The respective curves serve as an indicator of vortex shedding cycle status at the instantaneous point of time. They confirm the periodicity of numerical results in an unsteady flow regime. It is well-known that when the cylinder lies in an unconfined domain, the lift coefficient oscillates about zero periodically, as the vortex shedding occurs and a zero average lift coefficient prevails. When the cylinder is brought in the vicinity of a stationary wall, both C_D and C_L oscillate periodically, but not about zero, resulting in a non-zero average lift coefficient. A uniform swaying is seen in C_L curves, while C_D curves appear distorted, but the variation is still periodic. The abnormal patterns of C_D swaying for $C1$ and $C2$ configurations are a mirror image of each other as shown in subplot (i) of Fig. 3(a) and (b). Hence, the wall and orientation of the semi-circular cylinder affect the pressure distribution and the overall flow phenomenon. A detailed dialogue on the orientation effects is given in the sections to follow. Oscillation patterns of lift coefficient are similar for both $C1$ and $C2$ configurations. Both lift and drag coefficient values are higher for all G/D ratio values for $C2$ configuration. As the G/D ratio is decreased, the amplitude of C_L and C_D oscillations reduce, possibly due to

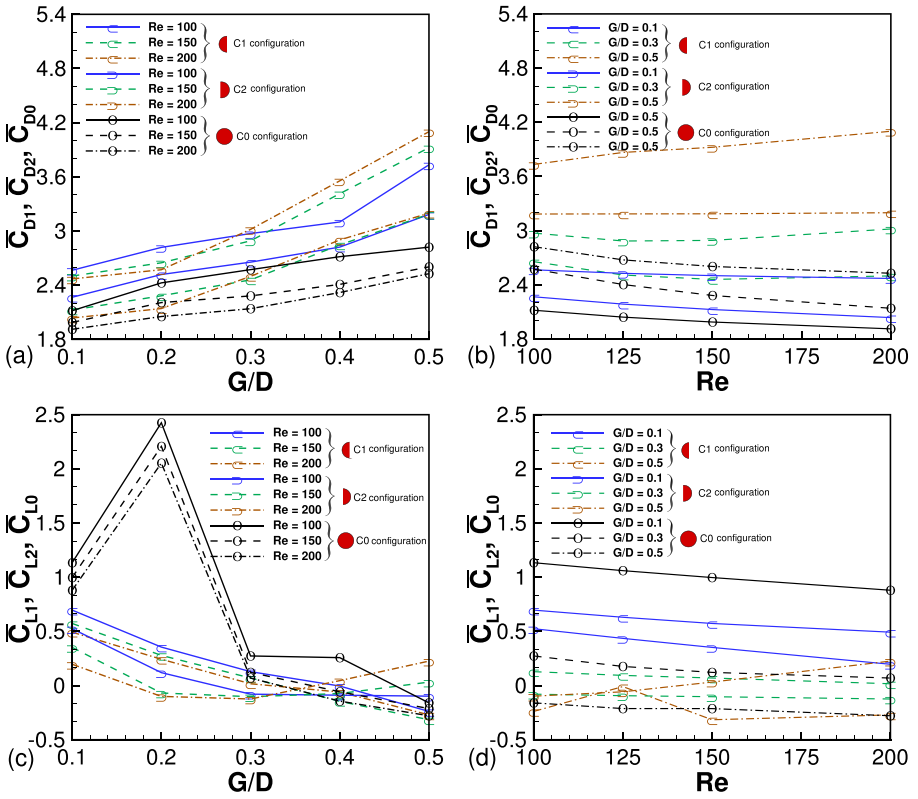

Fig. 5. Time-averaged drag ($\overline{C}_{D1}$, $\overline{C}_{D2}$ and $\overline{C}_{D0}$) and lift coefficient ($\overline{C}_{L1}$, $\overline{C}_{L2}$ and $\overline{C}_{L0}$ of $C1$, $C2$ and $C0$ configurations, respectively) of the cylinder as a function of (a,c) cylinder-to-wall gap ratio (G/D) and (b,d) Reynolds number (Re).

an adverse outcome of the interaction of the stationary wall. Below $G/D = 0.3$, no presence of vortex shedding is apparent, while both drag and lift coefficients monotonically increase. The suppression of vortex shedding can be seen clearly through the vorticity contours shown in Fig. 4.

5.1.2. Instantaneous vorticity contours: suppression of vortex shedding

For flow across a circular cylinder, in an unconfined domain, the shear layer around the body is made up of the boundary layer, separating the free shear layer and wake forming downstream. In the steady flow regime, *i.e.*, before vortex shedding occurs, the wake region contains a constant recirculation with two symmetrically placed standing vortices downstream of the body. Beyond a particular Re value, the downstream end of the recirculation bubble develops unsteadiness. As a result, alternate shedding of vortices occurs downstream of the cylinder, forming a typical von Kármán vortex street, as seen in Fig. 4(i). The occurrence of this street when the semi-circular cylinder is closer to the stationary wall (with decreasing G/D ratio values) is studied in the present study.

Instantaneous vorticity contours around the semi-circular cylinder is shown in Fig. 4. When the cylinder is brought near the wall, at high gap ratio values, sufficient momentum can be supplied to the wake region through the gap between cylinder and wall. Hence, vortex streets do exist behind the cylinder but are asymmetric, somewhat oblique due to interaction with the shear layer formed on the stationary wall (see Fig. 4(ii)). As the cylinder approaches the wall, at lower gap ratio values, flow between the semi-circular cylinder and wall crams like a jet flow. Ultimately, the lower separated shear layer of the cylinder is restricted from interacting with the upper shear layer of the cylinder. Thus, vortex shedding suppression occurs as the upper shear layer extends downstream without rolling up and the lower shear layer and wall boundary layer reunite at the cylinder flat face (or curved face), as shown in Fig. 4(iii) and (iv). Such occurrences are witnessed for other bluff body shapes as well. Perhaps the semi-circular cylinder is no exception for the fundamental flow physics that occurs when any bluff body is brought near the stationary wall under shear flow. Also, beyond $G/D = 0.3$, there exists no rolling up or shedding pattern of vortices as such. However, the exact details are given through the frequency of lift coefficient oscillations later.

One thing is clear that $C1$, $C2$, and, $C0$ configurations generally offer the same qualitative traits based on vorticity contours. Further, when the cylinder approaches the wall, a separation bubble oozes alternatively from the cylinder and moves downstream. This unsteady nature of the flow is termed vortex shedding, as stated earlier. Again, due to the interference of the shear layers of the cylinder and wall, these recirculation regions elongate downstream and merge at lower gap ratio values ($G/D \leq 0.3$). The outcome is an extended and standing detached recirculation region. The oblique nature seen in the vorticity field persists in streamlines due to wall shear layer presence.

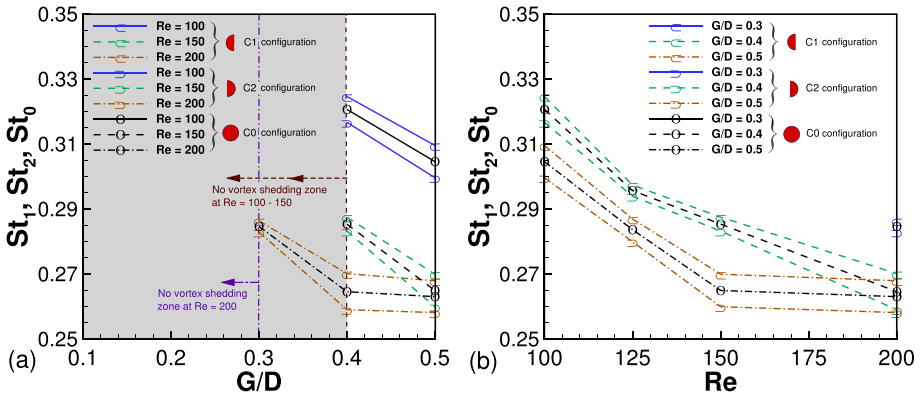

Fig. 6. Strouhal number (*i.e.*, St_1, St_2 and St_0 denoted for *C*1, *C*2 and *C*0 configurations, respectively) as a function of (*a*) cylinder-to-wall gap ratio (*G*/*D*) and (*b*) Reynolds number (*Re*).

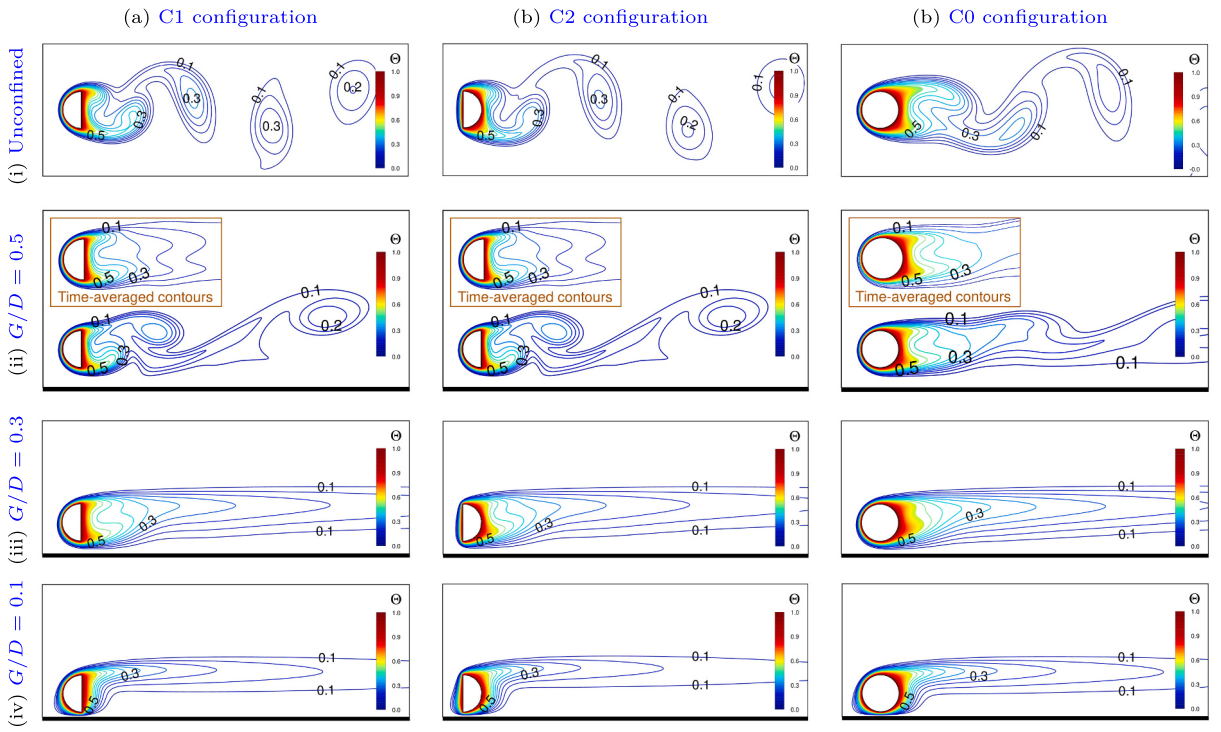

Fig. 7. Instantaneous isotherm contours in the wake of cylinder at different configurations for various cylinder-to-wall gap ratio (*G*/*D*) values. Time-averaged contours are given in subplot (*ii*) at $G/D = 0.5$. The instantaneous contours are presented at non-dimensional time (τ) = 300 and at Reynolds number (*Re*) = 100.

5.1.3. *Time-averaged drag and lift coefficients*

The variation of time-averaged drag coefficients $\overline{C}_{D1}$, $\overline{C}_{D2}$, and $\overline{C}_{D0}$ are given for *C*1, *C*2, and *C*0 configurations, respectively in Fig. 5. As seen earlier, as the gap between the cylinder and wall is reduced, suppression of vortex shedding occurs, indicating a strong influence of wall proximity on flow. Similar dominance can be seen in the drag and lift forces acting on the cylinder. As shown in Fig. 5 (b), with variation in *G*/*D* values, for a given value of *Re*, drag coefficient decreases with decreasing gap distance between cylinder and wall. Due to the blunt nature of the fore-body shape, drag force stays higher for the *C*2 configuration. Overall, it is observed that the placement of a wall near the bluff body results in the reduction of drag force acting on it. For a given *G*/*D* value, increasing Reynolds number does not seem to affect the drag coefficient significantly, as shown in Fig. 5(b). The order of drag coefficient magnitude is $C_{D2} \geq C_{D1} \geq C_{D0}$ for the considered range of parameters.

Similar to the drag coefficient, the time-averaged lift coefficient is also labelled after respective configurations, and its variation is displayed in Fig. 5(c) and (d). Lift coefficient variation differ due to the presence of the wall when compared with an unconfined

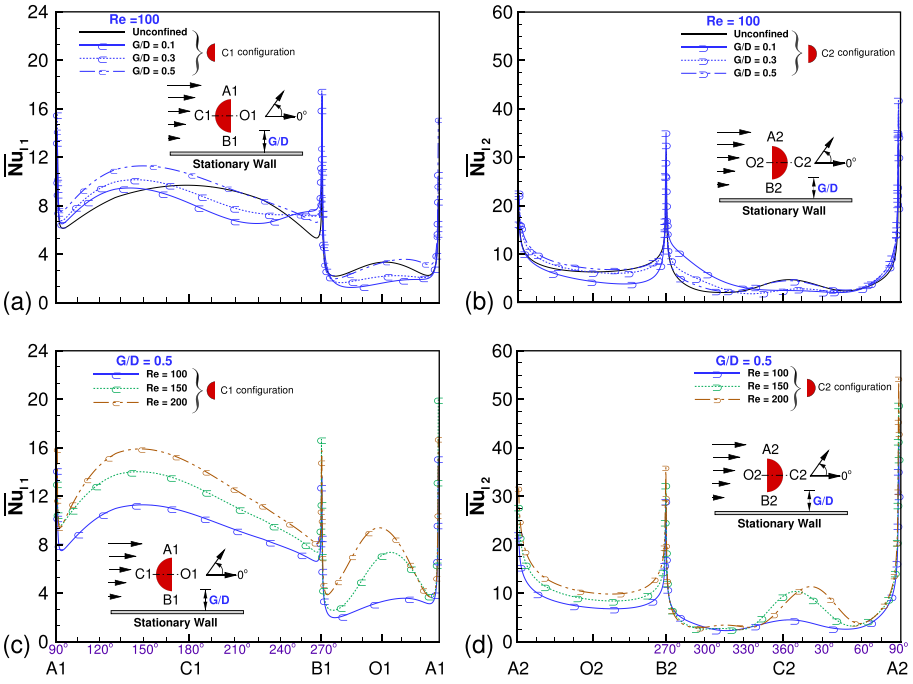

Fig. 8. Distribution of time-averaged local Nusselt number, $\overline{Nu}_{l\,1}$ and $\overline{Nu}_{l\,2}$ for $C1$ and $C2$ configurations, respectively. Plots (a) and (b) are shown at Reynolds number, Re = 100. Plots (c) and (d) are shown at cylinder-to-wall gap ratio, $G/D = 0.5$.

cylinder, where the magnitude of the average lift coefficient is zero. Rather, the wall imparts a positive thrust due to the gap flow on the cylinder as the gap ratio value decreases. This force decreases due to thinning of the viscous boundary layer as the Reynolds number is increased for a given value of G/D. It can be said that at intermediate G/D values, the semi-circular cylinder experiences a downforce because of the wall. Overall, the lift coefficient is higher for the $C0$ configuration, followed by $C1$ and $C2$ configurations.

5.1.4. Strouhal number

Strouhal number, St ($= fD/U_0$), is a non-dimensional parameter to measure the vortex shedding frequency of an oscillating flow, and it is obtained from the time evolution of the lift coefficient curve of the cylinder. The dependency of Strouhal number on G/D and Re is presented in Fig. 6. At moderate gap ratio values, before the suppression of vortex shedding, St increases as the semi-circular cylinder approaches the wall because of the acceleration of flow in the gap region. However, after a certain gap ratio, the jet flow overwhelms the interaction of the upper separated shear layer with other shear layers, and suppression of vortex shedding happens. After that, no variation in St can be seen. Also, if fluid momentum in such a gap flow regime is increased by increasing Re, a negative dependency on St is observed for moderate G/D ratio values. Such an occurrence suggests that the gap flow regime influences the occurrence of vortex shedding stronger than any other parameter. $(G/D)_{cr}$ values have been reported to be $G/D = 0.4$ for Re up to 150, while no vortex shedding is evident beyond $G/D = 0.3$ for Re = 200.

5.2. Heat transfer characteristics

5.2.1. Isotherms

Fig. 7 shows the instantaneous temperature contours, which correspond to the instantaneous vorticity contours shown in Fig. 4. The heat transfer from a semi-circular cylinder and the influence G/D ratio on it is explored for the first time. When the cylinder is far away from the stationary wall, the distribution of temperature-concentration on the surface of the cylinder corresponds to the distinct two-row street of vortices. Streamwise stretching of the thermal blobs from the $C0$ configuration appears more because of the greater surface area than other configurations and the absence of sharp edges. As the semi-circular cylinder is closer to the wall, isotherm contours stretch away from the lower sharp end of the cylinder (near the wall) and appear denser than the top sharp corner. Because of the interaction between positive and negative vortices emanating from the cylinder and wall surfaces, respectively, these vortices stretch away at the upper end and reattach to the cylinder near the wall. Similar enactment happens with the isotherm contours as well, resulting in a thinner thermal boundary layer at the top end and a thicker thermal boundary layer near the bottom end of the cylinder (near the wall) as shown in the plot of time-averaged contours Fig. 7(ii). However, at lower values of G/D, the reverse happens due to a single extended asymmetric recirculation region behind the cylinder. At this condition, the thermal boundary layer appears thinner near the wall end of the cylinder, while it is thick towards the upper end, away from the wall. Overall, the thermal boundary layer appears to be more thinner for $C1$ configuration compared to others. The influence of the fore-body shape seems less significant in

Table 2
Comparison of time averaged mean Nusselt number $\overline{Nu}_{M1}$, $\overline{Nu}_{M2}$ and $\overline{Nu}_{M0}$ values of the cylinder at various cylinder-to-wall gap ratio (G/D) and Reynolds number (Re) values.

$\overline{Nu}_M$	G/D	Re			
		100	125	150	200
$\overline{Nu}_{M1}$	0.1	5.863	6.309	6.742	7.611
	0.2	6.023	6.760	7.421	8.572
	0.3	6.484	7.230	8.073	9.847
	0.4	6.811	7.922	8.872	10.469
	0.5	7.340	8.387	9.298	10.925
$\overline{Nu}_{M2}$	0.1	5.093	5.368	5.649	6.236
	0.2	5.077	5.560	6.023	6.807
	0.3	5.262	5.753	6.312	7.377
	0.4	5.376	6.097	6.724	7.821
	0.5	5.682	6.385	7.014	8.109
$\overline{Nu}_{M0}$	0.1	5.573	5.896	6.600	7.204
	0.2	5.310	5.888	6.684	7.731
	0.3	5.681	6.353	7.202	8.180
	0.4	6.120	6.817	7.245	8.448
	0.5	6.423	7.283	8.236	9.600

thermal contour distribution, and G/D appears to have more weight.

5.2.2. Time-averaged local and mean Nusselt number variation

Time-averaged local Nusselt number distribution along the surface of the cylinder is shown in Fig. 8 and the influence of G/D and Re variation is shown. It is well established that because of the fresh incoming flow, the frontal surface of any bluff body displays maximum heat transfer and that the rear face provides comparatively low heat transfer (as the recirculation region exists here). The thermal boundary layer variation explained above agrees well with the shown distribution of local Nu, and the maximum Nu point on the frontal surface in both $C1$ and $C2$ configurations shifts away from the wall. Also, with a decrement in the G/D ratio, the maximum value decreases. For the $C1$ configuration, due to the higher surface area on the curved surface, overall higher heat transfer occurs than for $C2$. In the $C2$ configuration, the curved surface shows almost the same heat transfer as the flat frontal face. The fore-body shape does play a significant role in altering the thermal field across the heated semi-circular cylinder. However, for a given G/D ratio, a monotonous rise can be predicted in the mean Nusselt number after inspecting the local Nu variation. It is to be mentioned that the corners act as the starting point of the thermal boundary layer. Therefore, a sudden rise in local Nu values is obtained at these points because of high thermal gradients normal to the surface of the cylinder. For modelling this singularity nature at the corners, special emphasis was given to the grid size there.

Time-averaged mean Nusselt number comparison is provided in Table 2. Although the peak values at the corner of the semi-circular cylinder for $C2$ configuration rises well above $C1$, the overall average remains higher for the $C1$ configuration as the Nusselt number distribution on faces is higher for this setup. Overall, as predicted in the local Nusselt number distribution, the time-averaged mean Nusselt number decreases with decreasing G/D ratio it monotonously increases with Re. In spite of having a higher surface area, $C0$ configuration provides smaller heat transfer than $C1$ configuration, followed by $C2$ configuration. Hence, it is clear that the fore-body shape does affect flow and heat transfer and that a streamlined fore-body and blunt aft-body can provide better performance in heat dissipation. The blunt-aft body causes immediate rolling up of vortices behind the cylinder compared to streamlined fore-body, resulting in better heat dissipation. Such an aft-body may not be an ideal choice where flow stability is a significant concern, but this shape can serve better from the heat transport perspective.

Correlations based on the present results are proposed through curve fitting by using the multiple non-linear regression method. The functional dependence of the mean Nusselt number with Re and G/D are obtained for the chosen range of parameters,

$$(Nu_M)_1 = \Lambda Re^{1.134656} G/D^{0.4380301} + 4.115223, \tag{5}$$

$$(Nu_M)_2 = \Lambda Re^{1.0382912} G/D^{0.3064764} + 3.4762591, \text{and} \tag{6}$$

$$(Nu_M)_0 = \Lambda Re^{1.0382892} G/D^{0.3064694} + 3.4762605, \tag{7}$$

where $\Lambda = 0.023166$, and $G/D \leq 0.5$.

The above correlations have the correlation coefficient values of $R^2 = 0.991$, 0.961 and 0.989, respectively, and the maximum deviation is found to be 3.786%.

5.2.3. Enhancement in heat transfer

For highlighting the enhancement/decrement of time-averaged mean Nusselt number discussed above, enhancement ratio values are compared for different flow conditions and orientations of the semi-circular cylinder. A two-fold comparison is provided while discussing the enhancement ratio, one concerning shear flow (SF) with the uniform flow (UF) and the other concerning configurations

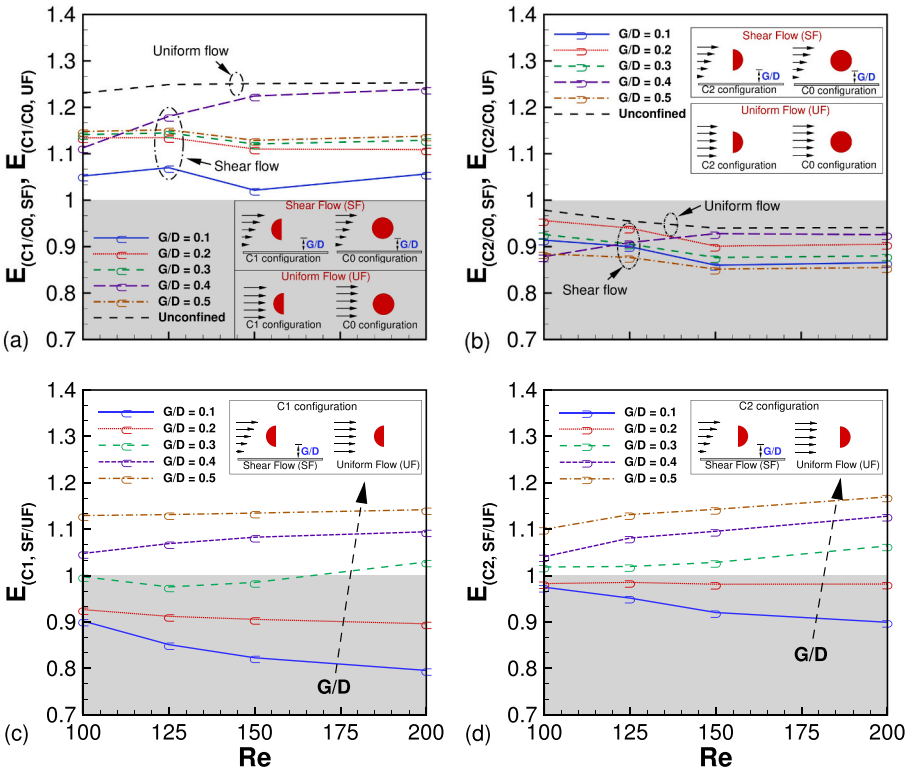

Fig. 9. Heat transfer enhancement ratio of (*a*) *C*1 and (*b*) *C*2 configurations with respect to *C*0 configuration under both shear (*i.e.*, $E_{(C1/C0,SF)}$ and $E_{(C2/C0,SF)}$) and uniform (*i.e.*, $E_{(C1/C0,UF)}$ flow conditions. Subplots (*c*) and (*d*) show heat transfer enhancement ratio for *C*1 and *C*2 configurations in shear flow with respect to uniform flow condition (*i.e.*, $E_{(C1,SF/UF)}$ and $E_{(C2,SF/UF)}$) at various Reynolds number (*Re*) values.

under the same type of flow. For instance, $E_{(C1/C0,SF)}$ represent enhancement ratio calculated for shear flow across *C*1 configuration with reference to *C*0, while $E_{(C2,SF/UF)}$ stands for enhancement ratio for shear flow with respect to uniform flow for *C*2 configuration as shown in Fig. 9 (a)-(d). Details on the relations used for calculating the enhancement ratios are given below,

$$E_{(C1/C0,UF)} = \frac{Nu_{(C1,UF)}}{Nu_{(C0,UF)}}, E_{(C2/C0,UF)} = \frac{Nu_{(C2,UF)}}{Nu_{(C0,UF)}}, \tag{8}$$

$$E_{(C1/C0,SF)} = \frac{Nu_{(C1,SF)}}{Nu_{(C0,SF)}}, E_{(C2/C0,SF)} = \frac{Nu_{(C2,SF)}}{Nu_{(C0,SF)}}, \tag{9}$$

$$E_{(C1,SF/UF)} = \frac{Nu_{(C1,SF)}}{Nu_{(C1,UF)}}, \text{and } E_{(C2,SF/UF)} = \frac{Nu_{(C2,SF)}}{Nu_{(C2,UF)}}. \tag{10}$$

Clearly, the *C*1 configuration shows enhancement in heat transfer with respect to the *C*0 configuration, while there is a decrement for the *C*2 configuration. Reynolds number variation more or less shows the same trends. However, with increasing *G/D* ratio, there is an increment in enhancement ratio values. Also, uniform flow or unconfined flow shows a better heat transfer rate than shear flow. Such a trend can be credited to smooth fluid flow across the curved surface of the semi-circular cylinder. Hence, it is clear that the *C*1 configuration provides a higher heat transfer rate in smooth flow concerning *C*0 configuration and that wall proximity decreases the same. On the other hand, the *C*2 configuration provides a smaller heat transfer rate in uninterrupted flow with respect to *C*0 configuration, and the wall proximity further decreases the same.

When uniform flow and linear shear flow are compared for *C*1, and *C*2 configurations, more surprising outcomes are unfolding. The heat transfer enhancement decreases for both the configurations when the cylinder moves towards the wall and this reduction is prominent for the *C*1 configuration. At $G/D = 0.3$, both uniform and shear flow conditions behave similarly, and any further decrease in gap ratio results in low enhancement ratio values. Again, Reynolds number increment shows an almost flat response on the curve trend, only at a lower *G/D* ratio values some decrement happens due to enhanced jet effect in the gap flow regime.

6. Conclusions

The prime aim of the study is to highlight the flow and forced convection heat transfer from a semi-circular cylinder under linear shear flow near a wall. Unsteady flow simulations are investigated for different ranges of Reynolds number ($100 \leq Re \leq 200$) and cylinder-to-wall gap ratio ($0.1 \leq G/D \leq 0.5$) values. An unsteady flow of Newtonian fluid with uniform properties has been studied. A comparison with the uniform flow is provided along with a discussion on flow and thermal fields of a circular cylinder ($C0$ configuration) concerning semi-circular cylinder orientations. Two distinct orientations of the semi-circular cylinder are focused on, *i.e.* rounded, and flat fore-bodies facing the incoming flow, and they are named as $C1$ and $C2$ configurations, respectively. Time-averaged lift coefficient, pressure coefficient, Strouhal number, and time-averaged mean Nusselt number are higher for $C1$ configuration, while the coefficient of drag is higher for $C2$ configuration. The proximity of a stationary wall in shear flow across the semi-circular cylinder results in suppression of vortex shedding. Critical value of G/D ratio for $\mathrm{Re} = 100$ to 150 is 0.4, while for $\mathrm{Re} = 200$ it is 0.3. Overall, the flow field across the semi-circular cylinder is qualitatively similar to its other cross-section counterparts. The presence of the wall affects the heat transfer from the hot semi-circular cylinder negatively. With decreasing G/D ratio, the time-averaged mean Nusselt number is decreases significantly. In conclusion, the $C1$ configuration provides higher heat transfer than both $C2$ and $C0$ configuration. Also, at moderate G/D ratio values ($G/D = 0.5$–0.3), shear flow performs better than uniform flow regarding heat dissipation. However, at lower gap ratios ($G/D \leq 0.3$), the converse is true. Correlations for time-averaged mean Nusselt number are given regarding operating parameters. In the future, a three-dimensional study can be carried out to model the current setup with better accuracy and to set up a guideline regarding the Reynolds number range to distinguish between 2D and 3D modelling.

References

[1] M. Taslim, Rib fin effects on the overall equivalent heat transfer coefficient in a rib-roughened cooling channel, Int. J. Heat Exch. 6 (2) (2005) 135.
[2] J. Hua, G. Li, X. Zhao, Q. Li, Experimental study on thermal performance of micro pin fin heat sinks with various shapes, Heat Mass Tran. 53 (3) (2017) 1093–1104.
[3] J.-H. Kim, Y.O. Han, Experimental investigation of wake structure around an external rear view mirror of a passenger car, J. Wind Eng. Ind. Aerod. 99 (12) (2011) 1197–1206.
[4] M. Mier-Torrecilla, E. Herrera, M. Doblaré, Numerical calculation of wind loads over solar collectors, Energy Procedia 49 (2014) 163–173.
[5] S. Sivakumar, K. Siva, M. Mohanraj, Experimental thermodynamic analysis of a forced convection solar air heater using absorber plate with pin-fins, J. Therm. Anal. Calorim. 136 (1) (2019) 39–47.
[6] R.A. Kumar, B.G. Babu, M. Mohanraj, Thermodynamic performance of forced convection solar air heaters using pin–fin absorber plate packed with latent heat storage materials, J. Therm. Anal. Calorim. 126 (3) (2016) 1657–1678.
[7] J. Welti-Chanes, J.F. Velez-Ruiz, Transport Phenomena in Food Processing, CRC Press, 2016.
[8] E. Kim, C. Oh, S. Sherman, Simplified optimum sizing and cost analysis for compact heat exchanger in VHTR, Nucl. Eng. Des. 238 (10) (2008) 2635–2647.
[9] S.K. Singh, M. Mishra, P. Jha, Nonuniformities in compact heat exchangers—scope for better energy utilization: a review, Renew. Sustain. Energy Rev. 40 (2014) 583–596.
[10] N. Boisaubert, M. Coutanceau, P. Ehrmann, Comparative early development of wake vortices behind a short semicircular-section cylinder in two opposite arrangements, J. Fluid Mech. 327 (1996) 73–99.
[11] A. Chandra, R. Chhabra, Flow over and forced convection heat transfer in Newtonian fluids from a semi-circular cylinder, Int. J. Heat Mass Tran. 54 (1) (2011) 225–241.
[12] A. Kumar, A. Dhiman, L. Baranyi, Fluid flow and heat transfer around a confined semi-circular cylinder: onset of vortex shedding and effects of Reynolds and Prandtl numbers, Int. J. Heat Mass Tran. 102 (2016) 417–425.
[13] A. Gode, A.K. Sahu, R. Chhabra, Two-dimensional steady flow over a semi-circular cylinder: drag coefficient and Nusselt number, International Journal of Advances in Engineering Sciences and Applied Mathematics 3 (1–4) (2011) 44–59.
[14] A.P.S. Bhinder, S. Sarkar, A. Dalal, Flow over and forced convection heat transfer around a semi-circular cylinder at incidence, Int. J. Heat Mass Tran. 55 (19) (2012) 5171–5184.
[15] M.K. Sukesan, A.K. Dhiman, Laminar mixed convection in a channel with a built-in semi-circular cylinder under the effect of cross-buoyancy, Int. Commun. Heat Mass Tran. 58 (2014) 25–32.
[16] D. Chatterjee, B. Mondal, P. Halder, Unsteady forced convection heat transfer over a semicircular cylinder at low Reynolds numbers, Numer. Heat Tran., Part A: Applications 63 (6) (2013) 411–429.
[17] D. Chatterjee, B. Mondal, Effect of thermal buoyancy on fluid flow and heat transfer across a semicircular cylinder in cross-flow at low Reynolds numbers, Numer. Heat Tran., Part A: Applications 67 (4) (2015) 436–453.
[18] A. YashodharaRao, A.S. Rao, A.S. Rao, Dynamics of fluid flow around aerofoil, and submarine: effect of winglets, Int. J. Eng. Sci. 2 (1) (2013) 39–46.
[19] C. Fureby, B. Anderson, D. Clarke, L. Erm, S. Henbest, M. Giacobello, D. Jones, M. Nguyen, M. Johansson, M. Jones, et al., Experimental and numerical study of a generic conventional submarine at 10° yaw, Ocean. Eng. 116 (2016) 1–20.
[20] S. Bhattacharyya, D. Maiti, Vortex Shedding from a square cylinder with ground effect, in: ASME/JSME 4th Joint Fluids Summer Engineering Conference vols. 95–100, American Society of Mechanical Engineers, 2003.
[21] S. Bhattacharyya, D. Maiti, Shear flow past a square cylinder near a wall, Int. J. Eng. Sci. 42 (19) (2004) 2119–2134.
[22] S. Bhattacharyya, D. Maiti, Vortex shedding suppression for laminar flow past a square cylinder near a plane wall: a two-dimensional analysis, Acta Mech. 184 (1) (2006) 15–31.
[23] D.K. Maiti, Dependence of flow characteristics of rectangular cylinders near a wall on the incident velocity, Acta Mech. 222 (3) (2011) 273–286.
[24] D.K. Maiti, Numerical study on aerodynamic characteristics of rectangular cylinders near a wall, Ocean. Eng. 54 (2012) 251–260.
[25] A. Dipankar, T. Sengupta, Flow past a circular cylinder in the vicinity of a plane wall, J. Fluid Struct. 20 (3) (2005) 403–423.
[26] M. Kumaran, S. Vengadesan, Flow characteristics behind rectangular cylinder placed near a wall, Numer. Heat Tran., Part A: Applications 52 (7) (2007) 643–660.
[27] A. Singha, A. Sarkar, P. De, Numerical study on heat transfer and fluid flow past a circular cylinder in the vicinity of a plane wall, Numer. Heat Tran., Part A: Applications 53 (6) (2007) 641–666.
[28] P. Scandura, V. Armenio, E. Foti, Numerical investigation of the oscillatory flow around a circular cylinder close to a wall at moderate Keulegan–Carpenter and low Reynolds numbers, J. Fluid Mech. 627 (2009) 259–290.
[29] N. Mahir, Three-dimensional flow around a square cylinder near a wall, Ocean. Eng. 36 (5) (2009) 357–367.
[30] D. Kumar, A. Dhiman, Computations of Newtonian fluid flow around a square cylinder near an adiabatic wall at low and intermediate Reynolds numbers: effects of cross-buoyancy mixed convection, Numer. Heat Tran., Part A: Applications 70 (2) (2016) 162–186.
[31] S. Kumarasamy, J.B. Barlow, Unsteady Flow over a Half Cylinder in Proximity to a Stationary and Moving Wall, Tech. Rep, SAE Technical Paper, 1996.
[32] S. Kumarasamy, J.B. Barlow, Computation of unsteady flow over a half-cylinder close to a moving wall, J. Wind Eng. Ind. Aerod. 69 (1997) 239–248.

[33] A. Kumar, A. Dhiman, L. Baranyi, CFD analysis of power-law fluid flow and heat transfer around a confined semi-circular cylinder, Int. J. Heat Mass Tran. 82 (2015) 159–169.
[34] S. Kang, Uniform-shear flow over a circular cylinder at low Reynolds numbers, J. Fluid Struct. 22 (4) (2006) 541–555.
[35] S. Dhinakaran, Heat transport from a bluff body near a moving wall at Re = 100, Int. J. Heat Mass Tran. 54 (25) (2011) 5444–5458.
[36] A.F. Ansys, 14.0 Theory Guide, ANSYS INC, 2011, pp. 218–221.
[37] S. Patankar, D. Spalding, A calculation procedure for heat, mass and momentum transfer in three-dimensional parabolic flows, Int. J. Heat Mass Tran. 15 (10) (1972) 1787–1806.
[38] B.P. Leonard, A stable and accurate convective modelling procedure based on quadratic upstream interpolation, Comput. Methods Appl. Mech. Eng. 19 (1) (1979) 59–98.
[39] S. Patankar, Numerical Heat Transfer and Fluid Flow, CRC press, 1980.
[40] C.H. Williamson, Oblique and parallel modes of vortex shedding in the wake of a circular cylinder at low Reynolds numbers, J. Fluid Mech. 206 (1989) 579–627.
[41] J. Park, K. Kwon, H. Choi, Numerical solutions of flow past a circular cylinder at Reynolds numbers up to 160, Korean Society of Mechanical Engineers International Journal 12 (6) (1998) 1200–1205.